

A rotating GUP black hole: metric, shadow, and bounds on quantum parameters

Federica Fragomeno,^a Samantha Hergott,^{b,e} Saeed Rastgoo,^{a,c,d} Evan Vienneau,^a

^a*Department of Physics, University of Alberta, Edmonton, Alberta T6G 2G1, Canada*

^b*Department of Physics and Astronomy, York University, Toronto, Ontario M3J 1P3, Canada*

^c*Department of Mathematical and Statistical Sciences, University of Alberta, Edmonton, Alberta T6G 2G1, Canada*

^d*Theoretical Physics Institute, University of Alberta, Edmonton, Alberta T6G 2G1, Canada*

^e*Perimeter Institute for Theoretical Physics, Waterloo, ON N2L 2Y5, Canada*

E-mail: ffragome@ualberta.ca, sherrgs@yorku.ca,
srastgoo@ualberta.ca, eviennea@ualberta.ca

ABSTRACT: Recently, for the first time, a metric of a static spherically symmetric generalized uncertainty inspired quantum black hole was derived. We apply the modified Newman-Janis algorithm to this metric and derive its rotating counterpart. We show that this metric has all the correct limits, while due to Newman-Janis side effects, the singularity which was resolved in the static case, is introduced back into the model. However, the slowly-rotating limit of this black hole is singularity-free. Furthermore, we show that the presence of quantum parameters modifies the location of the horizons, temperature, and entropy of the black hole, and allows the existence of naked singularities even if the ratio of the spin parameter to mass of the black hole is less than unity. Finally, by computing the shadow parameters of this black hole and comparing them with data from the Event Horizon Telescope for both M87* and Sgr A*, we set bounds on one of the quantum parameters of the model, and show that there is a limit on the angular momentum of M87* if this model is valid.

Contents

1	Introduction	1
2	Brief Overview Of The Modified Newman-Janis Algorithm	3
3	A GUP Rotating Black Hole Metric	5
3.1	The Full Metric	5
3.2	Horizons	7
3.3	Thermodynamics	9
3.4	The Fate of Singularity	11
3.4.1	Full Rotating Metric	11
3.4.2	Slowly-Rotating Metric	16
4	Shadow and Phenomenology	18
4.1	The Shape of the Shadow	18
4.2	Bounds on Quantum Parameter Q_b From Sgr A* And M87*	20
5	Conclusion	22
A	Estimating the Kretschmann of the full metric	23

1 Introduction

Black holes provide one of the most promising arenas to test quantum-gravity-inspired modifications of classical general relativity. Several approaches to quantum gravity have put forward models of quantum black holes [1] suggesting corrections that can soften or resolve the singularity in static, collapsing, and rotating geometries. There are also model-independent proposals showing these features for fully dynamical cases involving matter [2, 3]. These effects are also present in lower dimensional black holes (see, e.g., [4, 5]). In this context, generalized uncertainty principle (GUP) deformations offer a phenomenological framework in which short-distance quantum effects can be encoded in modified black hole metrics and observables [6–12].

Recently, a static spherically symmetric improved GUP black hole metric, possessing two quantum parameters Q_b and Q_c , was derived systematically [13, 14]. In

that construction, Q_b primarily controls near-horizon and exterior quantum corrections, whereas Q_c mainly affects the deep interior structure. A natural next step is to obtain the rotating counterpart of this static solution, since astrophysical black holes are expected to possess nonzero angular momentum. Hence, introducing rotation is crucial for confronting the model with observations.

To construct the rotating geometry, one method is to employ the Newman-Janis (NJ) algorithm [15], or modified variants of it [16–18]. However, the NJ procedure is known to be subtle beyond the original Kerr construction when the original equations of motion of the underlying theory are not known: depending on the seed metric and implementation details, it may generate geometries with nontrivial pathologies, and regularity properties of the static seed are not guaranteed to persist [19–22]. This motivates a careful analysis of the asymptotic and near-singularity limits, curvature behavior, and horizon structure in any NJ-generated rotating extension.

In this work, we apply a modified NJ algorithm to the improved static GUP black-hole metric introduced in [13] and derive its rotating version. We show that the resulting spacetime has the appropriate classical and nonrotating limits. We then study the horizon structure and extremality conditions, and show that the quantum effects can shift horizon radii and allow naked singularity configurations even for $\frac{a}{M} < 1$. We also compute thermodynamic quantities and find that quantum effects lower both the temperature and entropy compared with the classical rotating case.

We also investigate whether the model has a singularity, find that it does, and identify similar pathologies to those reported previously [19–22]. However, we show that the slowly-rotating limit is singularity-free.

Finally, we investigate observational signatures by computing the shadow of the rotating GUP black hole and comparing it with Event Horizon Telescope (EHT) measurements for M87* and Sgr A* [23–25]. From this comparison, we place bounds on the quantum parameter Q_b and identify an upper bound on the allowed spin of M87* within this model. These results provide a direct bridge between quantum gravity-motivated black hole geometry and current horizon scale observations.

The paper is organized as follows. In Sec. 2 we review the modified NJ algorithm used in our construction and present the general rotating metric associated to a static black hole. In Sec. 3 we present the rotating metric of the GUP rotating black hole and analyze its consistency by studying the asymptotic and classical limits. We also study the horizons, extremality condition, and thermodynamic properties of the black hole. Furthermore, we compute the Kretschmann scalar in both the fully rotating and slowly-rotating cases, and also find the affine distance to the $r = 0$ region. Sec. 4 is the phenomenological heart of the paper in which we compute the shadow of the black hole and derive constraints on its quantum parameters by comparing the model to the

EHT data from Sgr A* and M87*. Finally, we summarize our results and conclude in Sec. 5.

2 Brief Overview Of The Modified Newman-Janis Algorithm

The NJ algorithm [15] was introduced as a means to derive the Kerr metric from the static spherically symmetric Schwarzschild solution. Recently, a modified version of it was presented [16–18] in which the explicit complexification of the coordinates is avoided and instead certain other conditions are introduced to arrive at the final result (see below). Here we briefly describe this modified algorithm.

Consider the generic static spherically symmetric metric

$$ds^2 = g_{00}dt^2 + g_{11}dr^2 + g_{22}d\Omega^2, \quad (2.1)$$

where $d\Omega^2 = d\theta^2 + \sin^2(\theta)d\phi^2$ and hence $g_{33} = g_{22}\sin^2(\theta)$. In order to derive a rotating counterpart of this metric, one first transforms to the outgoing Eddington-Finkelstein (EF) coordinates

$$u = t - r^* = t - \int \sqrt{-\frac{g_{11}}{g_{00}}} dr, \quad (2.2)$$

where r^* is the radial tortoise coordinate. The metric is now

$$\begin{aligned} ds^2 &= g_{\tilde{0}\tilde{0}}^{(\text{EF})} du^2 + 2g_{\tilde{0}\tilde{1}}^{(\text{EF})} dudr + g_{\tilde{2}\tilde{2}}^{(\text{EF})} d\Omega^2 \\ &= g_{00} du^2 + 2\text{sgn}(g_{00}) \sqrt{-g_{00}g_{11}} dudr + g_{22} d\Omega^2, \end{aligned} \quad (2.3)$$

where $g_{\tilde{\mu}\tilde{\nu}}$ are the components of the metric in the EF coordinates. Using the Newman-Penrose formalism [26], the inverse of this metric

$$g^{(\text{EF})\tilde{0}\tilde{1}} = \frac{1}{g_{\tilde{0}\tilde{1}}^{(\text{EF})}}, \quad g^{(\text{EF})\tilde{1}\tilde{1}} = -\frac{g_{\tilde{0}\tilde{0}}^{(\text{EF})}}{\left[g_{\tilde{0}\tilde{1}}^{(\text{EF})}\right]^2} \quad (2.4)$$

$$g^{(\text{EF})\tilde{2}\tilde{2}} = \frac{1}{g_{\tilde{2}\tilde{2}}^{(\text{EF})}}, \quad g^{(\text{EF})\tilde{3}\tilde{3}} = \frac{1}{g_{\tilde{3}\tilde{3}}^{(\text{EF})}} \quad (2.5)$$

is now written in terms of four null tetrads $l^{\tilde{\mu}}, n^{\tilde{\mu}}, m^{\tilde{\mu}}, \bar{m}^{\tilde{\mu}}$, as

$$g^{(\text{EF})\tilde{\mu}\tilde{\nu}} = -l^{\tilde{\mu}}n^{\tilde{\nu}} - l^{\tilde{\nu}}n^{\tilde{\mu}} + m^{\tilde{\mu}}\bar{m}^{\tilde{\nu}} + m^{\tilde{\nu}}\bar{m}^{\tilde{\mu}} \quad (2.6)$$

where $l^{\tilde{\mu}}, n^{\tilde{\mu}}$ are real and $m^{\tilde{\mu}}$ is complex with its complex conjugate being $\bar{m}^{\tilde{\mu}}$, and they obey the normalization conditions

$$g_{\tilde{\mu}\tilde{\nu}}^{(\text{EF})} l^{\tilde{\mu}} n^{\tilde{\nu}} = -1, \quad g_{\tilde{\mu}\tilde{\nu}}^{(\text{EF})} m^{\tilde{\mu}} \bar{m}^{\tilde{\nu}} = 1 \quad (2.7)$$

with the rest of the inner products vanishing. From Eq. (2.6) and the above normalization conditions (and the null property of the tetrads) one can find them as

$$l^{\tilde{\mu}} = \delta_{\tilde{1}}^{\tilde{\mu}}, \quad (2.8)$$

$$n^{\tilde{\mu}} = \frac{1}{\sqrt{-g_{00}g_{11}}} \delta_{\tilde{0}}^{\tilde{\mu}} - \frac{1}{2g_{11}} \delta_{\tilde{1}}^{\tilde{\mu}}, \quad (2.9)$$

$$m^{\tilde{\mu}} = \frac{1}{(\sqrt{2g_{22}})^*} \delta_{\tilde{2}}^{\tilde{\mu}} \pm \frac{i}{\sin(\theta)} \frac{1}{(\sqrt{2g_{22}})^*} \delta_{\tilde{3}}^{\tilde{\mu}}, \quad (2.10)$$

$$\bar{m}^{\tilde{\mu}} = \frac{1}{(\sqrt{2g_{22}})^*} \delta_{\tilde{2}}^{\tilde{\mu}} \mp \frac{i}{\sin(\theta)} \frac{1}{(\sqrt{2g_{22}})^*} \delta_{\tilde{3}}^{\tilde{\mu}}. \quad (2.11)$$

In the original NJ algorithm for the Schwarzschild black hole, $\frac{1}{(\sqrt{2g_{22}})^*} = \frac{1}{\sqrt{2}r^*}$, and hence one complexifies r while keeping $n^{\tilde{\mu}}$ real. In the modified approach one avoids that step (see below for the conditions that replace this). Next, one introduces the angular momentum into the metric by performing a deformation transformation

$$r' = r + ia \cos(\theta), \quad \theta' = \theta, \quad (2.12)$$

$$u' = u - ia \cos(\theta), \quad \phi' = \phi. \quad (2.13)$$

At the same time, one assumes that under this transformation, the $g_{\mu\nu}(r)$ components become $\check{g}_{\mu\nu}(r, \theta, a)$. The condition replacing complexification is $\lim_{a \rightarrow 0} \check{g}_{\mu\nu} = g_{\mu\nu}$. The above transformation results in $g^{\mu'\nu'}$ from which one can find $g_{\mu'\nu'}$ as

$$\begin{aligned} ds'^{(\text{EF})} &= \check{g}_{00} du'^2 - 2\sqrt{-\check{g}_{00}\check{g}_{11}} du' dr' - 2a \sin^2(\theta) \left(\check{g}_{00} + \sqrt{-\check{g}_{00}\check{g}_{11}} \right) du' d\phi \\ &\quad + 2a \sin^2(\theta) \sqrt{-\check{g}_{00}\check{g}_{11}} dr' d\phi \\ &\quad + \check{g}_{22} d\theta^2 + \sin^2(\theta) \left[\check{g}_{22} + a^2 \sin^2(\theta) \left(\check{g}_{00} + 2\sqrt{-\check{g}_{00}\check{g}_{11}} \right) \right] d\phi^2. \end{aligned} \quad (2.14)$$

Note that all instances of $g_{\mu\nu}(r)$ are replaced by $\check{g}_{\mu\nu}(r, \theta, a)$. One now makes a transformation

$$du' = d\bar{t} + \lambda(\bar{r}) d\bar{r}, \quad dr' = d\bar{r} \quad (2.15)$$

$$d\phi = d\bar{\phi} + \chi(\bar{r}) d\bar{r}, \quad d\theta = d\bar{\theta} \quad (2.16)$$

to the Boyer-Lindquist (BL) coordinates. The reason λ and χ depend only on r is that if they also depended on θ and ϕ , the transformation would be invalid, and the NJ algorithm would fail to transform the metric into BL form. The unknowns $\lambda(\bar{r})$ and $\chi(\bar{r})$ are found using three criteria: 1) The BL conditions $g_{\bar{t}\bar{r}} = 0 = g_{\bar{r}\bar{\phi}}$. 2) the dependence of $\lambda(\bar{r})$ and $\chi(\bar{r})$ is solely on \bar{r} . 3) $\lim_{a \rightarrow 0} \check{g}_{\mu\nu} = g_{\mu\nu}$. Finding these

unknowns and replacing them back into the metric after the above transformation yields the rotating metric components

$$g_{\bar{0}\bar{0}} = - \frac{\check{g}_{22} \left[\frac{g_{22}}{g_{11}} + a^2 \cos^2(\theta) \right]}{\left[\frac{g_{22}}{\sqrt{-g_{00}g_{11}}} + a^2 \cos^2(\theta) \right]^2}, \quad (2.17)$$

$$g_{\bar{0}\bar{3}} = - a \sin^2(\theta) \check{g}_{22} \frac{\frac{g_{22}}{\sqrt{-g_{00}g_{11}}} - \frac{g_{22}}{g_{11}}}{\left[\frac{g_{22}}{\sqrt{-g_{00}g_{11}}} + a^2 \cos^2(\theta) \right]^2}, \quad (2.18)$$

$$g_{\bar{1}\bar{1}} = \frac{\check{g}_{22}}{\frac{g_{22}}{g_{11}} + a^2}, \quad (2.19)$$

$$g_{\bar{2}\bar{2}} = \check{g}_{22}, \quad (2.20)$$

$$g_{\bar{3}\bar{3}} = \check{g}_{22} \sin^2(\theta) \left[1 + a^2 \sin^2(\theta) \left(\frac{a^2 \cos^2(\theta) - \frac{g_{22}}{g_{11}} + 2 \frac{g_{22}}{\sqrt{-g_{00}g_{11}}}}{\left[\frac{g_{22}}{\sqrt{-g_{00}g_{11}}} + a^2 \cos^2(\theta) \right]^2} \right) \right]. \quad (2.21)$$

Notice that this algorithm does not fix \check{g}_{22} . This can be fixed by requiring that the classical and nonrotating limits match their expected limits (see below), which yields

$$\check{g}_{22} = g_{22} + a^2 \cos^2(\theta). \quad (2.22)$$

It is worth noting that there exists another method of obtaining a slowly-rotating metric from the static one [27, 28], which in our case can simply be obtained by taking the $a^2 \rightarrow 0$ limit of the above metric but keeping the terms first order in a .

3 A GUP Rotating Black Hole Metric

3.1 The Full Metric

Using the result of the previous section and the components of the static GUP inspired quantum black hole derived in [13],

$$g_{00}(r) = - \left(1 + \frac{Q_b}{r^2} \right) \left(1 + \frac{Q_c R_s^2}{4r^8} \right)^{-\frac{1}{4}} \left(1 - \frac{R_s}{\sqrt{r^2 + Q_b}} \right), \quad (3.1)$$

$$g_{11}(r) = \left(1 + \frac{Q_c R_s^2}{4r^8} \right)^{\frac{1}{4}} \left(1 - \frac{R_s}{\sqrt{r^2 + Q_b}} \right)^{-1}, \quad (3.2)$$

$$g_{22}(r) = r^2 \left(1 + \frac{Q_c R_s^2}{4r^8} \right)^{\frac{1}{4}}, \quad (3.3)$$

$$g_{33}(r) = r^2 \left(1 + \frac{Q_c R_s^2}{4r^8} \right)^{\frac{1}{4}} \sin^2(\theta), \quad (3.4)$$

and following the method presented in the previous section, the NJ-rotated version of the static GUP metric is obtained as

$$g_{\bar{0}\bar{0}} = -\frac{\rho^2}{\Sigma^2} (\Sigma - \Lambda), \quad (3.5)$$

$$g_{\bar{0}\bar{3}} = -\frac{a \sin^2(\theta) \rho^2}{\Sigma^2} \Lambda, \quad (3.6)$$

$$g_{\bar{1}\bar{1}} = \frac{\rho^2}{\Delta}, \quad (3.7)$$

$$g_{\bar{2}\bar{2}} = \rho^2, \quad (3.8)$$

$$g_{\bar{3}\bar{3}} = \frac{\rho^2 \sin^2(\theta)}{\Sigma^2} [\Sigma^2 + a^2 \sin^2(\theta) (\Sigma + \Lambda)], \quad (3.9)$$

where

$$\rho^2 = \check{g}_{22} = g_{22} + a^2 \cos^2(\theta) = r^2 \left(1 + \frac{Q_c R_s^2}{4r^8} \right)^{\frac{1}{4}} + a^2 \cos^2(\theta), \quad (3.10)$$

$$\Delta = \frac{g_{22}}{g_{11}} + a^2 = r^2 \left(1 - \frac{R_s}{\sqrt{r^2 + Q_b}} \right) + a^2, \quad (3.11)$$

$$\Sigma = \frac{g_{22}}{\sqrt{-g_{00}g_{11}}} + a^2 \cos^2(\theta) = (\rho^2 - a^2 \cos^2(\theta)) \left(1 + \frac{Q_b}{r^2} \right)^{-\frac{1}{2}} + a^2 \cos^2(\theta), \quad (3.12)$$

$$\Lambda = \Sigma - \Delta + a^2 \sin^2(\theta). \quad (3.13)$$

A plot of these metric components for certain values of parameters is depicted in Fig. 1.

We notice from (3.10)-(3.16) that for the classical limit where $Q_b, Q_c \rightarrow 0$ we get

$$\rho_{\text{class}}^2 = r^2 + a^2 \cos^2(\theta), \quad (3.14)$$

$$\Delta_{\text{class}} = r^2 \left(1 - \frac{R_s}{r} \right) + a^2, \quad (3.15)$$

$$\Sigma_{\text{class}} = \rho^2. \quad (3.16)$$

In the same way, for the nonrotating (and also slowly-rotating) limit we obtain

$$\rho_{\text{NR}}^2 = r^2 \left(1 + \frac{Q_c R_s^2}{4r^8} \right)^{\frac{1}{4}}, \quad (3.17)$$

$$\Delta_{\text{NR}} = r^2 \left(1 - \frac{R_s}{\sqrt{r^2 + Q_b}} \right), \quad (3.18)$$

$$\Sigma_{\text{NR}} = \rho^2 \left(1 + \frac{Q_b}{r^2} \right)^{-\frac{1}{2}}, \quad (3.19)$$

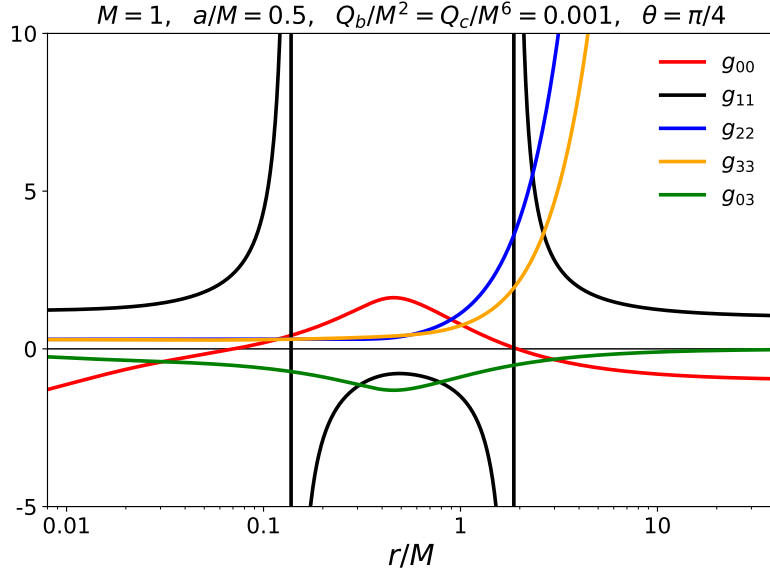


Figure 1. Plot of rotating GUP metric components in Schwarzschild coordinates with the given values of parameters on the top of the plot.

and in the combined classical and nonrotating limit we get

$$\rho_{\text{class-NR}}^2 = r^2, \quad (3.20)$$

$$\Delta_{\text{class-NR}} = r^2 \left(1 - \frac{R_s}{r} \right), \quad (3.21)$$

$$\Sigma_{\text{class-NR}} = r^2. \quad (3.22)$$

The above results show that the classical limit of the metric is the Kerr metric, the nonrotating limit is the static GUP metric (3.1)-(3.4) and the classical nonrotating case reduces to the Schwarzschild metric as it should.

One can also check that the asymptotic expansion of the metric components behave as they should. In particular, they reduce to the Kerr components for $Q_b, Q_c \rightarrow 0$ and to the Schwarzschild case for $a \rightarrow 0$ and $Q_b, Q_c \rightarrow 0$.

3.2 Horizons

As usual, the horizons of such a black hole can be derived by setting $g^{11} = 0$, which corresponds to

$$\Delta(r) = r^2 \left(1 - \frac{R_s}{\sqrt{r^2 + Q_b}} \right) + a^2 = 0. \quad (3.23)$$

Since this is a quadratic equation and also as can be seen from Fig. 2, $\Delta(r)$ admits at most two roots corresponding to an outer and an inner horizon. The inner and outer horizon radii can be obtained perturbatively by solving $\Delta = 0$ to first order in the parameter Q_b ,

$$r_- = \frac{1}{2} \left(R_s - \sqrt{R_s^2 - 4a^2} \right) + \frac{Q_b R_s}{R_s \left(\sqrt{R_s^2 - 4a^2} - R_s \right) + 4a^2}, \quad (3.24)$$

$$r_+ = \frac{1}{2} \left(R_s + \sqrt{R_s^2 - 4a^2} \right) - \frac{Q_b R_s}{R_s \left(\sqrt{R_s^2 - 4a^2} + R_s \right) - 4a^2}. \quad (3.25)$$

As expected, in the limit $Q_b \rightarrow 0$ these expressions smoothly reduce to the Kerr horizons. The quantum parameter shrinks the outer horizon and expands the inner horizon relative to their classical values. Since both ends of the function $\Delta(r)$ are positive, i.e., $\Delta(r \rightarrow 0) \rightarrow a^2 > 0$ and $\Delta(r \rightarrow \infty) \sim r^2 + a^2 > 0$, the horizons will only exist if there is a minimum of $\Delta(r)$ where $\Delta(r) \leq 0$. The extremal case happens when this root just touches the r axis, namely there is a degenerate root of $\Delta(r)$, in which case the two horizons coincide. This condition means the extremal horizon located at r_E happens when

$$\Delta(r_E) = 0 \quad \Delta'(r_E) = 0, \quad (3.26)$$

where

$$\Delta'(r) = 2r - \frac{R_s r (r^2 + 2Q_b)}{(r^2 + Q_b)^{3/2}}. \quad (3.27)$$

The resulting extremality relations are

$$R_s = \frac{2(r_E^2 + Q_b)^{\frac{3}{2}}}{r_E^2 + 2Q_b} \quad a_E^2 = \frac{r_E^4}{r_E^2 + 2Q_b} \approx \frac{R_s^2}{4} - 2Q_b, \quad (3.28)$$

where a_E^2 is the extremal spin parameter such that for $a^2 < a_E^2$ there are two horizons, for $a^2 = a_E^2$ there is one horizon (extremal case), and for $a^2 > a_E^2$ there are no horizons (naked singularity). The above approximation is valid for $Q_b \ll R_s$. In this limit, we obtain

$$r_E \approx \sqrt{\frac{R_s^2}{4} - Q_b}. \quad (3.29)$$

As a consistency check, in the classical limit, $Q_b \rightarrow 0$, we recover $a_E = \frac{R_s}{2}$, exactly as in Kerr. This suggests that Q_b lowers the maximum allowed spin for which horizons exist, as reflected in the condition $a_E^2 < r_E^2$. As mentioned above, for spins exceeding this extremal value $a^2 > a_E^2$, the minimum of $\Delta(r_E)$ remains positive and we do not have any horizons.

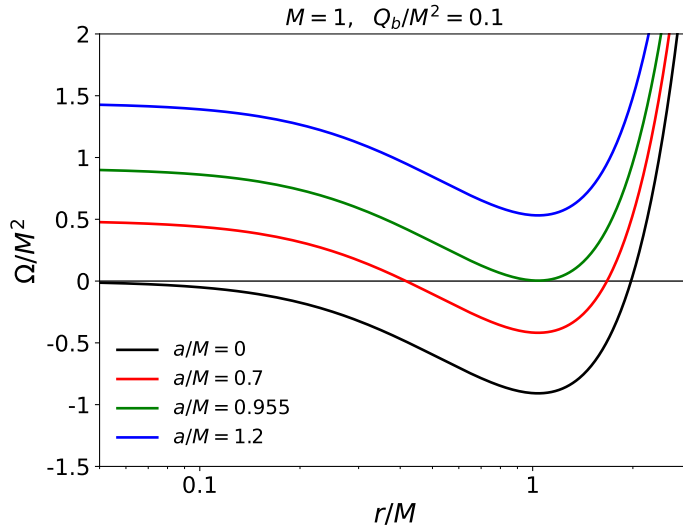


Figure 2. Plot of the horizon function, $\Omega(r)$, for several values of the spin parameter a , with the given value of parameters on the top of the plot.

Figure 3 shows the positions of inner and outer horizons as a function of the spin parameter a for various values of the quantum parameter Q_b , for a black hole with $M = 1$. As usual, for a nonrotating black hole, there is no inner horizon and the position of the single horizon decreases with increasing Q_b . For a rotating black hole, the distance between inner and outer horizons decrease with increasing a . Furthermore, the value of a at which the inner and outer horizons merge into one decreases with increasing Q_b . Notably, a nonzero value of Q_b allows for an extremal black hole to exist for $\frac{a}{M} < 1$, suggesting that in this model, naked singularities (if a singularity exists) can reasonably exist for specific parameter values.

3.3 Thermodynamics

For stationary, axisymmetric spacetimes written in BL-like coordinates, the surface gravity κ at the outer event horizon r_+ is determined by the radial derivative of the horizon function $\Delta(r)$ as

$$\kappa = \frac{\Delta'(r_+)}{2(r_+^2 + a^2)}.$$

The Hawking temperature is directly proportional to this surface gravity as

$$T_H = \frac{\kappa}{2\pi} = \frac{\Delta'(r_+)}{4\pi(r_+^2 + a^2)}. \quad (3.30)$$

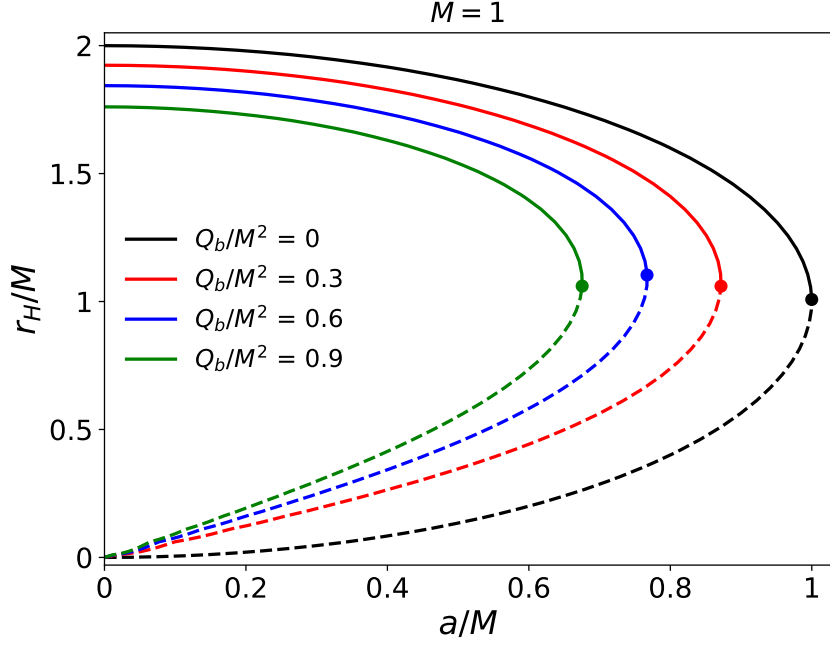


Figure 3. Plot which shows the radial positions of inner (dashed colored lines) and outer (solid colored lines) horizons for an $M = 1$ black hole, as a function of the spin parameter a for different values of the quantum parameter Q_b . Coloured points indicate the radii at which the inner and outer horizons merge to form one horizon, yielding an extremal black hole.

Replacing (3.27) in the above expression, and noting that at the horizon

$$\Delta(r_+) = 0 \Rightarrow \frac{R_s}{\sqrt{r_+^2 + Q_b}} = \frac{r_+^2 + a^2}{r_+^2}, \quad (3.31)$$

the temperature equation simplifies to

$$T_H = \frac{2r_+}{4\pi(r_+^2 + a^2)} - \frac{r_+^2 + 2Q_b}{4\pi r_+(r_+^2 + Q_b)}. \quad (3.32)$$

This reduces to the correct classical limit for $Q_b \rightarrow 0$, and furthermore shows that the temperature is lower than in the classical case due to quantum effects. From (3.30), it is clear that in the extremal case where $\Delta'(r_E) = 0 = \Delta(r_E)$ at the horizon, the temperature is zero as it should be for an extremal black hole.

For the entropy, we assume that the system still obeys

$$S = \frac{A}{4}, \quad (3.33)$$

where A is the area of the outer horizon. The area of r_+ is derived from the determinant of the $\theta - \phi$ block as

$$A = \int_0^{2\pi} \int_0^\pi \sqrt{g_{\theta\theta}g_{\phi\phi} - g_{\theta\phi}^2} d\theta d\phi = 4\pi (r_+^2 + a^2). \quad (3.34)$$

Hence, the entropy is

$$S = \pi (r_+^2 + a^2) \quad (3.35)$$

which is smaller than the classical case given that r_+ is smaller in the GUP case compared to its classical counterpart.

3.4 The Fate of Singularity

To study the behavior of the singularity and whether it is resolved, we consider both the Kretschmann scalar K and the affine parameters of suitable null geodesics reaching $r = 0$ from a larger r . Computing K yields a complicated expression, so instead we use an approximate method to estimate K near $r \rightarrow 0$ in the equatorial plane $\theta = \frac{\pi}{2}$. We consider the case of both the full metric and the slowly-rotating limit.

3.4.1 Full Rotating Metric

To compute the dominant term of the Kretschmann scalar K near $r \rightarrow 0$ and at $\theta = \frac{\pi}{2}$, we need the leading terms of the Riemann tensor components. We compute these components using Cartan's second structure equation. This requires the spin connection, which in turn is obtained from diagonal dual tetrads. The latter can be read off from the metric if we write it in a "diagonalized form".

To follow this procedure, we note that at $\theta = \frac{\pi}{2}$ and near $r \rightarrow 0$ we have

$$\rho^2|_{r \rightarrow 0} = \rho_0^2 + \mathcal{O}(r^8), \quad (3.36)$$

$$\Delta|_{r \rightarrow 0} = a^2 + \mathcal{O}(r^2), \quad (3.37)$$

$$\Sigma|_{r \rightarrow 0} = \rho_0^2 \frac{r}{\sqrt{Q_b}} + \mathcal{O}(r^3), \quad (3.38)$$

$$\Lambda|_{r \rightarrow 0} = \rho_0^2 \frac{r}{\sqrt{Q_b}} - a^2 + \mathcal{O}(r^2). \quad (3.39)$$

where

$$\rho_0^2 = \left(\frac{Q_c R_s^2}{4} \right)^{\frac{1}{4}}. \quad (3.40)$$

So the dominant terms of metric components in this approximation are

$$g_{\bar{0}\bar{0}}|_{r \rightarrow 0} \approx -\frac{Q_b}{\rho_0^2} \left(1 - \frac{R_s}{\sqrt{Q_b}}\right), \quad (3.41)$$

$$g_{\bar{0}\bar{3}}|_{r \rightarrow 0} \approx -\frac{a\sqrt{Q_b}}{r}, \quad (3.42)$$

$$g_{\bar{1}\bar{1}}|_{r \rightarrow 0} \approx \frac{\rho_0^2}{a^2}, \quad (3.43)$$

$$g_{\bar{2}\bar{2}}|_{r \rightarrow 0} \approx \rho_0^2, \quad (3.44)$$

$$g_{\bar{3}\bar{3}}|_{r \rightarrow 0} \approx \rho_0^2 + 2a^2 \frac{\sqrt{Q_b}}{r}, \quad (3.45)$$

For future reference, one can check that the inverse metric components' dominant behaviors are

$$g^{\bar{0}\bar{0}}|_{r \rightarrow 0} \approx \mathcal{O}(r), \quad (3.46)$$

$$g^{\bar{0}\bar{3}}|_{r \rightarrow 0} \approx \mathcal{O}(r), \quad (3.47)$$

$$g^{\bar{1}\bar{1}}|_{r \rightarrow 0} \approx \mathcal{O}(1), \quad (3.48)$$

$$g^{\bar{2}\bar{2}}|_{r \rightarrow 0} \approx \mathcal{O}(1), \quad (3.49)$$

$$g^{\bar{3}\bar{3}}|_{r \rightarrow 0} \approx \mathcal{O}(r^2) \quad (3.50)$$

We now use $g_{ab} = \eta_{IJ} e_a^I e_b^J$, where I, J are the $so(1,3)$ internal indices and assume diagonal dual tetrads to find e_a^I from

$$ds^2 = -(e^0)^2 + (e^1)^2 + (e^2)^2 + (e^3)^2. \quad (3.51)$$

In this last equation, indices are associated to $so(1,3)$. To achieve this, we need to diagonalize the line element. Since there are no cross terms $dr dx^\mu$, $\mu \neq r$ and $d\theta dx^\mu$, $\mu \neq \theta$ in the metric, we only need to diagonalize the $t - \phi$ part of the metric which at the moment looks like

$$ds_{t\phi}^2 = g_{\bar{0}\bar{0}} dt^2 + 2g_{\bar{0}\bar{3}} dt d\phi + g_{\bar{3}\bar{3}} d\phi^2. \quad (3.52)$$

Writing this metric as

$$ds_{t\phi}^2 = g_{33} \left(d\phi^2 + 2\frac{g_{03}}{g_{33}} dt d\phi \right) + g_{00} dt^2 \quad (3.53)$$

and completing the square for the parenthesis term, we obtain the full metric as

$$ds^2 = -\left(\frac{g_{\bar{0}\bar{3}}^2}{g_{\bar{3}\bar{3}}} - g_{\bar{0}\bar{0}}\right) dt^2 + g_{\bar{1}\bar{1}} dr^2 + g_{\bar{2}\bar{2}} d\theta^2 + g_{\bar{3}\bar{3}} \left(d\phi + \frac{g_{\bar{0}\bar{3}}}{g_{\bar{3}\bar{3}}} dt\right)^2. \quad (3.54)$$

The ratio $-\frac{g_{03}}{g_{33}}$ is sometimes referred to as the frame-dragging angular velocity of the spacetime. Comparing this form of the metric with (3.51) and our components (3.41)-(3.45), we can read off the dual tetrads as (we have suppressed the abstract indices a, b, \dots)

$$e^0 = \sqrt{\frac{g_{03}^2}{g_{33}} - g_{00}} dt \approx \left(\frac{\sqrt{Q_b}}{2r}\right)^{\frac{1}{2}} dt \quad (3.55)$$

$$e^1 = \sqrt{g_{11}} dr \approx \frac{\rho_0}{a} dr \quad (3.56)$$

$$e^2 = \sqrt{g_{22}} d\theta \approx \rho_0 d\theta \quad (3.57)$$

$$e^3 = \sqrt{g_{33}} \left(d\phi + \frac{g_{03}}{g_{33}} dt \right) \approx a \sqrt{\frac{2}{r}} Q_b^{\frac{1}{4}} \left(d\phi - \frac{1}{2a} dt \right) \quad (3.58)$$

where in computing e^0 and e^3 above, we have neglected the $\mathcal{O}(1)$ term g_{00} , and, in g_{33} , the $\mathcal{O}(1)$ term ρ_0^2 , keeping only $g_{33} \approx 2a^2 \frac{\sqrt{Q_b}}{r}$. We can invert the above equations and write down the coordinate basis one forms as

$$dt = \left(\frac{\sqrt{Q_b}}{2r}\right)^{-\frac{1}{2}} e^0, \quad (3.59)$$

$$dr = \frac{a}{\rho_0} e^1, \quad (3.60)$$

$$d\theta = \frac{1}{\rho_0} e^2, \quad (3.61)$$

$$d\phi = \frac{1}{a} (Q_b)^{-\frac{1}{4}} \sqrt{\frac{r}{2}} (e^3 + e^0). \quad (3.62)$$

In order to find the spin connection 1-form $\omega^I{}_J$ we use the torsionless Carter's first structure equation

$$de^I + \omega^I{}_J \wedge e^J = 0. \quad (3.63)$$

Thus, we need the exterior derivatives de^I . From (3.59)-(3.62) we see that $de^1 = 0 = de^2$, while the nonzero components become

$$de^0 = -\frac{1}{2} \left(\frac{\sqrt{Q_b}}{2r^3}\right)^{\frac{1}{2}} dr \wedge dt = \frac{a}{2r\rho_0} e^0 \wedge e^1, \quad (3.64)$$

$$de^3 = \sqrt{\frac{1}{2r^3}} Q_b^{\frac{1}{4}} \left(-a dr \wedge d\phi + \frac{1}{2} dr \wedge dt \right) = \frac{a}{2r\rho_0} e^3 \wedge e^1. \quad (3.65)$$

Matching the above result with Eq. (3.63), we obtain

$$\omega^0{}_1 = \omega^1{}_0 = -\frac{a}{2r\rho_0} e^0, \quad (3.66)$$

$$\omega^3{}_1 = -\omega^1{}_3 = -\frac{a}{2r\rho_0} e^3. \quad (3.67)$$

Next, we use the second Cartan's structure equation

$$R^I{}_J = d\omega^I{}_J + \omega^I{}_K \wedge \omega^K{}_J, \quad (3.68)$$

to find the components of the curvature 2-form. The nonvanishing terms are

$$R^0{}_1 = -\frac{3}{4} \frac{a^2}{r^2 \rho_0^2} e^0 \wedge e^1, \quad (3.69)$$

$$R^0{}_3 = -\frac{1}{4} \frac{a^2}{r^2 \rho_0^2} e^0 \wedge e^3, \quad (3.70)$$

$$R^1{}_3 = -\frac{3}{4} \frac{a^2}{r^2 \rho_0^2} e^1 \wedge e^3. \quad (3.71)$$

From this we can find the components of the Riemann tensor (since the tetrads are diagonal) as

$$R^0{}_{101} = -\frac{3}{4} \frac{a^2}{r^2 \rho_0^2}, \quad (3.72)$$

$$R^0{}_{303} = -\frac{1}{4} \frac{a^2}{r^2 \rho_0^2}, \quad (3.73)$$

$$R^1{}_{313} = -\frac{3}{4} \frac{a^2}{r^2 \rho_0^2}. \quad (3.74)$$

Finally, the Kretschmann scalar is obtained as

$$\begin{aligned} K &= R^{IJKL} R_{IJKL} \\ &= 4 (R^{0101} R_{0101} + R^{0303} R_{0303} + R^{1313} R_{1313}) \\ &= \frac{19}{2} \frac{a^4}{\sqrt{Q_c} R_s} \frac{1}{r^4}, \end{aligned} \quad (3.75)$$

where we have used (3.40). This is a softer singularity compared to the classical Kerr black hole that goes as r^{-6} , but it is still divergent.

Let us now study the affine parameter distance to $r = 0$. Considering a null geodesic $ds^2 = 0$ with $\theta = \frac{\pi}{2}$, from the line element we obtain

$$0 = g_{00} \dot{t}^2 + 2g_{03} \dot{t} \dot{\phi} + g_{33} \dot{\phi}^2 + g_{11} \dot{r}^2, \quad (3.76)$$

where the dots denote derivatives with respect to the affine parameter λ . The two Killing vector fields $\mathcal{K}^{\bar{\mu}} = \partial_0^{\bar{\mu}}$ and $\mathcal{R}^{\bar{\mu}} = \partial_3^{\bar{\mu}}$ of this spacetime lead to the invariant energy E and angular momentum L

$$E = -g_{\bar{\mu}\bar{\nu}} \mathcal{K}^{\bar{\mu}} \dot{x}^{\bar{\nu}} = -g_{00} \dot{x}^0 - g_{03} \dot{x}^3 = -g_{00} \dot{t} - g_{03} \dot{\phi} \quad (3.77)$$

$$L = g_{\bar{\mu}\bar{\nu}} \mathcal{R}^{\bar{\mu}} \dot{x}^{\bar{\nu}} = g_{03} \dot{x}^0 + g_{33} \dot{x}^3 = g_{03} \dot{t} + g_{33} \dot{\phi} \quad (3.78)$$

of the infalling object along the geodesic. The solution to these are

$$\dot{t} = -\frac{-Eg_{\bar{3}\bar{3}} - Lg_{\bar{0}\bar{3}}}{g_{\bar{0}\bar{3}}^2 - g_{\bar{0}\bar{0}}g_{\bar{3}\bar{3}}} \approx -\frac{-\mathcal{O}(r^{-1})E - \mathcal{O}(r^{-1})L}{\mathcal{O}(r^{-2}) - \mathcal{O}(r^{-1})} \approx \mathcal{O}(r), \quad (3.79)$$

$$\dot{\phi} = -\frac{Eg_{\bar{0}\bar{3}} + Lg_{\bar{0}\bar{0}}}{g_{\bar{0}\bar{3}}^2 - g_{\bar{0}\bar{0}}g_{\bar{3}\bar{3}}} \approx -\frac{\mathcal{O}(r^{-1})E - \mathcal{O}(1)L}{\mathcal{O}(r^{-2}) - \mathcal{O}(r^{-1})} \approx \mathcal{O}(r). \quad (3.80)$$

Substituting these into the null condition $ds^2 = 0$, we obtain

$$\begin{aligned} 0 &= g_{\bar{0}\bar{0}}\dot{t}^2 + 2g_{\bar{0}\bar{3}}\dot{t}\dot{\phi} + g_{\bar{3}\bar{3}}\dot{\phi}^2 + g_{\bar{1}\bar{1}}\dot{r}^2 \\ &\approx \mathcal{O}(1)\mathcal{O}(r^2) + \mathcal{O}(r^{-1})\mathcal{O}(r^2) + \mathcal{O}(r^{-1})\mathcal{O}(r^2) + g_{\bar{1}\bar{1}}\dot{r}^2 \\ &\approx \mathcal{O}(r^2) + \mathcal{O}(r) + \mathcal{O}(r) + g_{\bar{1}\bar{1}}\dot{r}^2. \end{aligned} \quad (3.81)$$

For $r \rightarrow 0$, the leading order behavior is therefore

$$g_{\bar{1}\bar{1}}\dot{r}^2 \approx \mathcal{O}(r), \quad (3.82)$$

and since $g_{\bar{1}\bar{1}} \approx \mathcal{O}(1)$ we get

$$\dot{r}^2 \sim r. \quad (3.83)$$

This leads to

$$\frac{dr}{d\lambda} \sim r^{\frac{1}{2}}, \quad (3.84)$$

and as a result

$$\Delta\lambda \sim \int_{r_0}^0 r^{-\frac{1}{2}} dr \sim \sqrt{r_0}. \quad (3.85)$$

Hence, $K(r \rightarrow 0) \rightarrow \infty$ while $r = 0$ can be reached in finite affine parameter. This implies that the ring singularity in this model is still present at $r = 0$, $\theta = \frac{\pi}{2}$. This seems to be a property of some of the rotating black hole models that are derived using the NJ algorithm. In these models, although the static regular black hole seed can be nonsingular, applying the NJ algorithm does not generically preserve all desirable properties and can reintroduces Kerr-like pathologies (including singular behavior, energy-condition violations, or naked-singularity branches), depending on the construction [19–22]. However, we will show in the next section that the slowly-rotating version of this metric avoids this singularity.

3.4.2 Slowly-Rotating Metric

As previously discussed, the slowly-rotating limit of this metric is the $a^2 \rightarrow 0$ limit of the full metric. It has a much simpler form and can be written as

$$g_{\bar{0}\bar{0}}^{(\text{slow})} = g_{00}(r), \quad (3.86)$$

$$g_{\bar{0}\bar{3}}^{(\text{slow})} = -a \sin^2(\theta) \left[\left(1 + \frac{Q_b}{r^2} \right)^{\frac{1}{2}} + g_{00}(r) \right], \quad (3.87)$$

$$g_{\bar{1}\bar{1}}^{(\text{slow})} = g_{11}(r), \quad (3.88)$$

$$g_{\bar{2}\bar{2}}^{(\text{slow})} = g_{22}(r), \quad (3.89)$$

$$g_{\bar{3}\bar{3}}^{(\text{slow})} = g_{33}(r). \quad (3.90)$$

It is seen that the only difference between the slowly-rotating GUP metric (3.86)-(3.90) and the static GUP metric (3.1)-(3.4) is the presence of $g_{\bar{0}\bar{3}}^{(\text{slow})}$ component, while all other metric components are the same.

A similar computation to the previous section reveals that the Kretschmann scalar in this case is finite and becomes $K = \frac{8}{R_s \sqrt{Q_c}}$. We can also show that it takes infinite affine parameter to reach $r = 0$. In this case, Eqs. (3.79) and (3.80) reduce to

$$\dot{t} = - \frac{-E g_{\bar{3}\bar{3}}^{(\text{slow})} - L g_{\bar{0}\bar{3}}^{(\text{slow})}}{\left[g_{\bar{0}\bar{3}}^{(\text{slow})} \right]^2 - g_{\bar{0}\bar{0}}^{(\text{slow})} g_{\bar{3}\bar{3}}^{(\text{slow})}} \approx - \frac{-\mathcal{O}(1) E - \mathcal{O}(r^{-1}) L}{\mathcal{O}(r^{-2}) - \mathcal{O}(1)} \approx \mathcal{O}(r), \quad (3.91)$$

$$\dot{\phi} = - \frac{E g_{\bar{0}\bar{3}}^{(\text{slow})} + L g_{\bar{0}\bar{0}}^{(\text{slow})}}{\left[g_{\bar{0}\bar{3}}^{(\text{slow})} \right]^2 - g_{\bar{0}\bar{0}}^{(\text{slow})} g_{\bar{3}\bar{3}}^{(\text{slow})}} \approx - \frac{\mathcal{O}(r^{-1}) E - \mathcal{O}(1) L}{\mathcal{O}(r^{-2}) - \mathcal{O}(r^{-1})} \approx \mathcal{O}(r). \quad (3.92)$$

Replacing these back into the null condition $ds^2 = 0$, we obtain

$$\begin{aligned} 0 &= g_{\bar{0}\bar{0}}^{(\text{slow})} \dot{t}^2 + 2g_{\bar{0}\bar{3}}^{(\text{slow})} \dot{t} \dot{\phi} + g_{\bar{3}\bar{3}}^{(\text{slow})} \dot{\phi}^2 + g_{\bar{1}\bar{1}}^{(\text{slow})} \dot{r}^2 \\ &\approx \mathcal{O}(1) \mathcal{O}(r^2) + \mathcal{O}(r^{-1}) \mathcal{O}(r^2) + \mathcal{O}(1) \mathcal{O}(r^2) + g_{\bar{1}\bar{1}} \dot{r}^2 \\ &\approx \mathcal{O}(r^2) + \mathcal{O}(r) + \mathcal{O}(r^2) + g_{\bar{1}\bar{1}} \dot{r}^2. \end{aligned} \quad (3.93)$$

For $r \rightarrow 0$, the leading order behavior is still

$$g_{\bar{1}\bar{1}}^{(\text{slow})} \dot{r}^2 \approx \mathcal{O}(r). \quad (3.94)$$

However, in this case we have $g_{\bar{1}\bar{1}}^{(\text{slow})} \approx \mathcal{O}(r^{-2})$ and hence

$$\dot{r}^2 \sim r^3. \quad (3.95)$$

This leads to

$$\frac{dr}{d\lambda} \sim r^{\frac{3}{2}}, \quad (3.96)$$

and as a result

$$\Delta\lambda \sim \int_{r_0}^0 r^{-\frac{3}{2}} dr \sim \left[\frac{1}{\sqrt{r}} \right]_{r_0}^0 \sim \infty. \quad (3.97)$$

Thus the singularity is actually resolved in the slowly-rotating metric. A physical interpretation of the fact that the singularity is resolved in the slowly-rotating case but not in the fully rotating scenario is that the slow-rotation limit effectively creates a logarithmic throat geometry, which explains both the infinite affine parameter and the very strong curvature divergence we computed earlier. To see the existence of this wormhole-like geometry, we check the proper radial distance and the area of the 2-spheres as $r \rightarrow 0$. If the proper distance diverges while the angular area approaches a finite non-zero value, the geometry develops a cylindrical (or infinite) throat.

For the proper radial distance we have

$$\begin{aligned} \ell(r) &= \int_{r_0}^0 \sqrt{g_{\text{II}}^{(\text{slow})}} dr \\ &\sim \int_{r_0}^0 \sqrt{r^{-2}} dr \\ &\sim [\ln(r)]_{r_0}^0 \\ &\sim \infty. \end{aligned} \quad (3.98)$$

So the first condition

$$\ell(r \rightarrow 0) \rightarrow \infty, \quad (3.99)$$

is satisfied. The second condition can be easily verified by considering the area of the 2-spheres

$$A = 4\pi \sqrt{g_{22}^{(\text{slow})} g_{33}^{(\text{slow})}} \approx \mathcal{O}(1). \quad (3.100)$$

Since the angular area approaches a finite, nonzero value as $r \rightarrow 0$ the second condition is also satisfied. Furthermore, a coordinate transformation

$$r = e^{-\ell} \quad (3.101)$$

near $r \rightarrow 0$ casts the rr , $\theta\theta$, and $\phi\phi$ part of the metric into

$$ds^2 \approx d\ell^2 + R_0^2 d\Omega^2, \quad (3.102)$$

which is the metric of a cylindrical throat.

In hindsight, one can argue that the slowly-rotating metric is closer to the static metric in which the singularity is resolved. So it seems that the NJ algorithm introduces the singularity back into the full rotating metric by structurally shearing the regularized core at the equator.

4 Shadow and Phenomenology

4.1 The Shape of the Shadow

With the rotating metric in hand, we are now interested in comparing the shadow of this black hole with observations from the Event Horizon Telescope (EHT) of the black hole at the center of our galaxy, Sgr A*, and the one at the heart of the M87 galaxy, known as M87*.

Rotating black holes do not have a photon sphere, instead they have a photon region. There is a counter-rotating circular orbit in the equatorial plane of the black hole at r_-^{ph} and a co-rotating circular orbit in the equatorial plane of the black hole at r_+^{ph} . The light rays in between these two orbits are non-planar and spherical (move on a spherical shell). We have $r_-^{\text{ph}} > r_+^{\text{ph}}$ and the region between these two which includes the non-planar spherical light orbits is called the photon region. Imagine a black hole rotating counter clockwise with respect to us, i.e., such that its left side is coming towards us and its right side going away from us. Then the light from the left side that we see coming towards us is emanating from r_+^{ph} and the light from the right side is coming from r_-^{ph} . The shadow is the boundary of past oriented light rays emanated from the observer that asymptotically end up on unstable spherical orbits around the black hole. Due to the fact that this boundary on the left and right is associated to rays that do not have the same orbit radius as mentioned above, the shadow of a rotating black hole is not a circle; it is oblique [29]. The spherical null geodesic that is the limiting curve for these past oriented light ray that emanated from the observer must have the same constants of motion L , E , i.e., angular momentum and energy respectively, which are determined by its radius r_p .

The contour of the rotating black hole shadow can be obtained by finding the unstable circular orbit of null geodesics, as outlined in Refs. [29–31]. The apparent shape of the shadow as seen by an observer located at asymptotically flat infinity, with an inclination angle θ_0 is given by the celestial coordinates α, β given by [29]

$$\alpha(r_p) = -\xi(r_p) \csc(\theta_0), \quad (4.1)$$

$$\beta(r_p) = \pm \sqrt{\eta(r_p) + a^2 \cos^2(\theta_0) - \xi(r_p)^2 \cot^2(\theta_0)}. \quad (4.2)$$

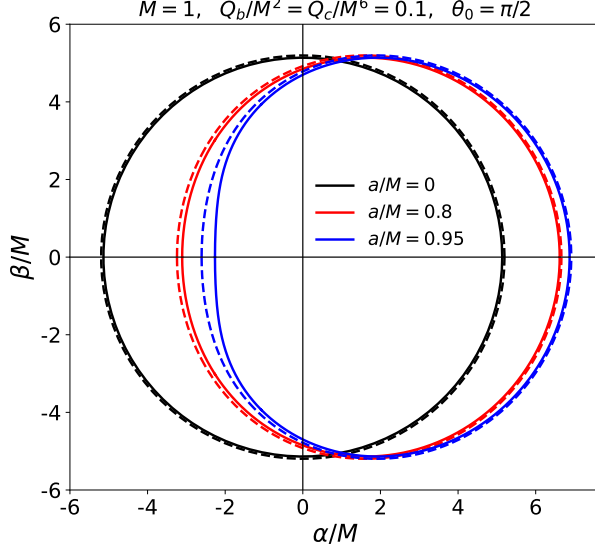


Figure 4. Shadow contours in celestial coordinates for three values of the spin parameter, $\frac{a}{M} = 0$ (black lines), $\frac{a}{M} = 0.8$ (red lines) and $\frac{a}{M} = 0.95$ (blue lines). Solid lines correspond to the shadow for this rotating GUP black hole with quantum parameters $\frac{Q_b}{M^2} = 0.1 = \frac{Q_c}{M^6}$, dashed lines correspond to the respective Kerr black hole ($\frac{Q_b}{M^2} = 0 = \frac{Q_c}{M^6}$). The black hole mass is $M = 1$ and the inclination angle is $\theta_0 = \frac{\pi}{2}$.

These are computed using the impact parameters for unstable circular photon orbits, given by

$$\xi(r_p) = \frac{\Upsilon(r_p) \Delta'(r_p) - 2\Delta(r_p) \Upsilon'(r_p)}{a\Delta'(r_{ps})} \quad (4.3)$$

$$\eta(r_p) = \frac{4a^2\Upsilon'(r_p)^2 \Delta(r_p) - [(\Upsilon(r_p) - a^2) \Delta'(r_p) - 2\Upsilon'(r_p) \Delta(r_p)]^2}{a^2\Delta'(r_p)} \quad (4.4)$$

where the prime denotes the derivative with respect to the radial coordinate r , and $\Upsilon(r)$ is given by

$$\Upsilon = \Sigma + a^2 \sin^2(\theta). \quad (4.5)$$

Furthermore, the first impact parameter $\xi = \frac{L}{E}$, is the photon's perpendicular distance from the rotation axis of the black hole as seen by a distant observer, and the second impact parameter, $\eta = \frac{\mathcal{K}}{E}$, measures the motion out of the equatorial plane. Here \mathcal{K} is the Carter constant.

Fig. 4 shows the black hole shadow contours in celestial coordinates for three values of the spin parameter, for this GUP rotating black hole with $\frac{Q_b}{M^2} = 0.1 = \frac{Q_c}{M^6}$ (solid

lines) and the corresponding classical Kerr black hole (dashed lines). The impact of the quantum parameter Q_b becomes larger as the spin of the black hole increases, with the largest deviation between the quantum and classical shadows appearing on the distorted side of the shadow.

4.2 Bounds on Quantum Parameter Q_b From Sgr A* And M87*

We now make use of shadow observables to constrain the quantum parameter Q_b . The other parameter Q_c has a much smaller effect on the shadow and contributes mostly to the quantum effects in the interior of the black hole, particularly near the singularity. The shadows of the Sgr A* and M87* black holes have been observed by the EHT [23, 25]. These observations provide measurements of the angular shadow diameter d_{sh} and Schwarzschild shadow deviation δ defined as

$$d_{\text{sh}} = \frac{2}{D} \sqrt{\frac{A}{\pi}}, \quad (4.6)$$

$$\delta = \frac{d_{\text{sh}}}{d_{\text{Sch}}} - 1, \quad (4.7)$$

where D is the distance from the observer to the black hole, d_{Sch} is the corresponding Schwarzschild angular shadow diameter of the black hole (i.e., for $a = 0$), and A is the shadow area defined as

$$A = 2 \int_{r_p^-}^{r_p^+} \beta(r_p) \frac{d\alpha(r_p)}{dr_p} dr_p. \quad (4.8)$$

Here r_p^- and r_p^+ are the minimal and maximal values of r_p , respectively [29].

For Sgr A*, EHT measures the angular shadow diameter to be $d_{\text{sh, SgrA}^*} = 48.7 \pm 7.0 \mu\text{as}$, using solely EHT data [25]. They obtain two measurements for the Schwarzschild shadow deviation using two different distance measurements as priors. We will consider the Schwarzschild shadow deviation measurement of $\delta_{\text{SgrA}^*} = -0.08 \pm 0.09$, which utilizes the most recent distant measurement of $D_{\text{SgrA}^*} = 8.277 \pm 0.033 \text{ kpc}$, as obtained from Very Large Telescope Interferometer observations of stellar orbits [32]. Both of the above shadow observables are given at the 1σ confidence level. For the mass of Sgr A*, we use the value as measured by [32], given by $M_{\text{SgrA}^*} = (4.297 \pm 0.013) \times 10^6 M_{\odot}$. The inclination angle of Sgr A* has been constrained to lie in the range of 40 - 60 deg. We consider the median value of $\theta_0 = 50 \text{ deg}$.

For M87*, EHT measures the angular shadow diameter to be in the range of $39 \mu\text{as} \lesssim d_{\text{sh, M87}^*} \lesssim 45 \mu\text{as}$ and the Schwarzschild shadow deviation to be $\delta_{\text{M87}^*} = -0.01 \pm 0.17$, at the 1σ confidence level [23, 24]. These observations are based on a distance of $D_{\text{M87}^*} = 16.8 \text{ Mpc}$ and an estimated mass of $M_{\text{M87}^*} = (6.5 \pm 0.7) \times 10^9 M_{\odot}$.

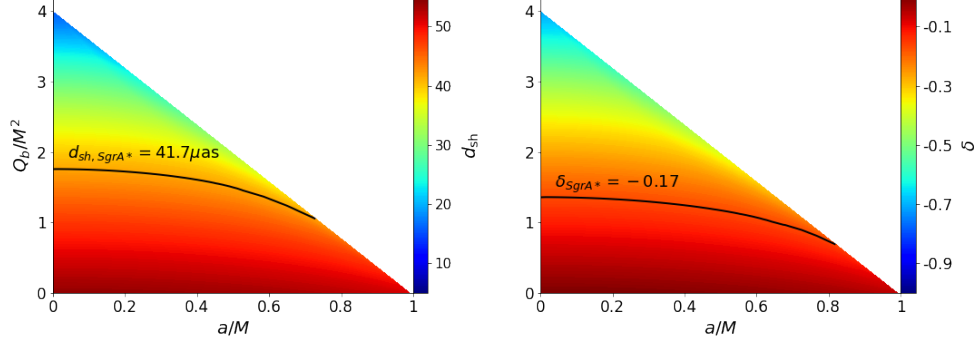


Figure 5. Angular shadow diameter d_{sh} (left plot) and Schwarzschild shadow deviation δ (right plot) for a range of quantum parameter Q_b values and spin parameter a values for the Sgr A* black hole, which has a mass, distance and inclination angle as given in the text. The solid black lines indicate the lower bounds on the values of d_{sh} and δ , respectively, for Sgr A* as measured from EHT observations. The white region shows the values of Q_b and a for which the black hole has no horizons.

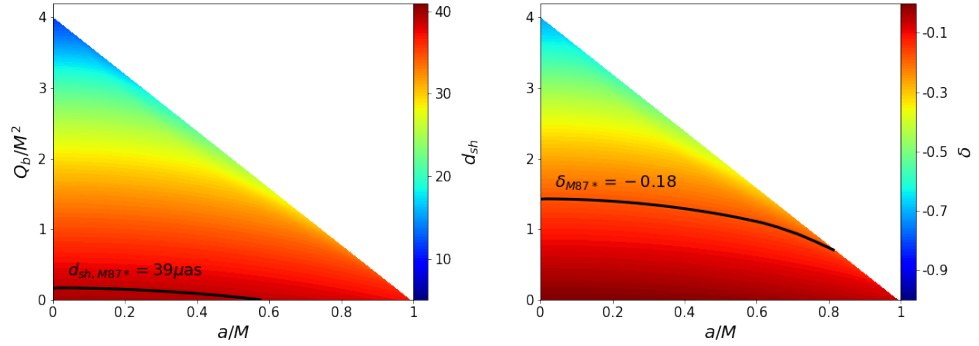


Figure 6. Same as Fig. 5 but for the M87* black hole, which has a mass, distance and inclination angle as given in the text. The solid black lines indicate the lower bounds on the values of d_{sh} and δ , respectively, for M87* as measured from EHT observations.

The inclination angle of M87* has been constrained to $\theta_0 \sim 17$ deg, which we use in our analysis.

Figs. 5 and 6 show the angular shadow diameter d_{sh} (left plot) and Schwarzschild shadow deviation δ (right plot) for a range of quantum parameter values Q_b , and spin parameter values a the Sgr A* (Fig. 5) and M87* (Fig. 6), respectively. The solid black lines indicate the lower bounds on the values of d_{sh} and δ , for each respective black hole. Any (a, Q_b) point that lies above the solid black lines is ruled out as a result of

these observations. The strongest constraint comes from the angular shadow diameter of M87* which requires $\frac{Q_b}{M^2} \lesssim (0.001 \sim 0.2)$ if M87* has a spin of $a/M < 0.6$. If M87* has a spin of $\frac{a}{M} < 0.6$, then $\frac{Q_b}{M^2}$ must be zero in order to be in agreement with EHT observations.

An interesting observation from Fig. 6 is that if this model is correct and if the numerical values of the observations are accurate, then this quantum black hole cannot rotate faster than $\frac{a}{M} \approx 0.6$. If an observed angular momentum of this black hole exceeds this value, it provides grounds for refuting this model.

5 Conclusion

In this work we have derived the metric for a rotating improved GUP black hole by applying the modified NJ algorithm to a recent metric of a static improved GUP black hole. Both these static and rotating models have two quantum parameters Q_b and Q_c . The former is the main contributor to quantum gravity effects near the horizon and outside of the black hole while the latter contributes to the interior modification and quantum effects near $r = 0$.

The result of application of the NJ algorithm is a spinning black hole that still has a maximum of two horizons, while the quantum parameter Q_b expands the inner horizon and shrinks the outer one. In the extremal case the radius of the only horizon is smaller than its classical counterpart and quantum effects allow a naked singularity for values of $\frac{a}{M}$ smaller than one.

Although the singularity was resolved in the static case, the rotation introduces it back into this rotating model. This is a rather well-known side effect of the Newman-Janis algorithm. The slowly-rotating version of this black hole, however, is singularity free, both due to the finiteness of the Kretschmann scalar and that the $r = 0, \theta = \frac{\pi}{2}$ region lies at infinite affine parameter.

We also compute the temperature and entropy of this black hole and show that they both are smaller compared to the classical case due to quantum effects associated with Q_b .

An important part of this investigation is comparing the model with observational data from the EHT. We have derived the shadow of this black hole and by comparing it to the EHT, we set strong bounds on the quantum parameter Q_b , i.e., $\frac{Q_b}{M^2} \lesssim (0.001 \sim 0.2)$ if M87* has a spin of $\frac{a}{M} < 0.6$. Furthermore, we show that if our model is valid and if the EHT data is accurate, the M87* black hole cannot rotate faster than $\frac{a}{M} \approx 0.6$. However, the data is still at the 1σ confidence level.

Acknowledgments

The authors acknowledge the support of the Natural Sciences and Engineering Research Council of Canada (NSERC). We also thank Douglas Gingrich for valuable discussions.

A Estimating the Kretschmann of the full metric

We have seen that the dominant order of the metric, its derivatives, and its inverse are

$$g \approx \mathcal{O}(r^{-1}), \quad \partial_r g \approx \mathcal{O}(r^{-2}), \quad g^{-1} \approx \mathcal{O}(1).$$

Consequently the Christoffel symbols behave as

$$\Gamma \approx g^{-1} \partial_r g \approx \mathcal{O}(1) \mathcal{O}(r^{-2}) \approx \mathcal{O}(r^{-2}), \quad (\text{A.1})$$

This is also because the dominant terms in Γ is g^{11} (of $\mathcal{O}(1)$); also g^{22} does not matter since $\partial_2 g$ vanishes for $\theta = \pi/2$, which is contracted by the dominant terms $\partial_1 g_{03}$ and $\partial_1 g_{03}$ (of $\mathcal{O}(r^{-2})$). The Riemann tensor as

$$R \approx \partial_r \Gamma + \Gamma^2 \approx \mathcal{O}(r^{-3}), \quad (\text{A.2})$$

since as mentioned above, the dominant terms of Γ are Γ_{33}^1 and Γ_{03}^1 but they should be contracted in the Riemann tensor as $\Gamma_{\mu\lambda}^\rho \Gamma_{\nu\sigma}^\lambda$. But any Γ with a lower index of 1 (e.g., $\Gamma_{\mu 1}^\rho$) is at most $\mathcal{O}(r^{-1})$, so Γ^2 goes as $\mathcal{O}(r^{-3})$ and not $\mathcal{O}(r^{-4})$.

To check the order of the Kretschmann scalar, we note that the severe divergences in the Riemann tensor come from the t and ϕ indices (indices 0 and 3). To raise these indices when calculating $K = R^{\alpha\beta\gamma\delta} R_{\alpha\beta\gamma\delta}$, we are forced to use $g^{00} \approx \mathcal{O}(r)$, $g^{03} \approx \mathcal{O}(r)$, and $g^{33} \approx \mathcal{O}(r^2)$. Contracting $\mathcal{O}(r^{-3})$ of the Riemann tensor with the dominant one of them, say g^{00} , yields $\mathcal{O}(r^{-2})$ and thus

$$K \approx (g^{-1})^4 R^2 \approx \mathcal{O}(r^{-4}). \quad (\text{A.3})$$

This is the same result we obtained before using the diagonal tetrad framework.

References

- [1] C. Bambi, ed., *Regular Black Holes: Towards a New Paradigm of Gravitational Collapse*. Springer, 2023.
- [2] S. Hergott, V. Husain and S. Rastgoo, *Model metrics for quantum black hole evolution: Gravitational collapse, singularity resolution, and transient horizons*, *Phys. Rev. D* **106** (2022) 046012 [[2206.06425](#)].

- [3] S. Hergott, V. Husain and S. Rastgoo, *Dynamical model for black hole to white hole transitions*, *Phys. Rev. D* **113** (2026) 024049 [[2505.15096](#)].
- [4] R. Gambini, J. Pullin and S. Rastgoo, *New variables for 1+1 dimensional gravity*, *Class. Quant. Grav.* **27** (2010) 025002 [[0909.0459](#)].
- [5] A. Corichi, J. Olmedo and S. Rastgoo, *Callan-Giddings-Harvey-Strominger vacuum in loop quantum gravity and singularity resolution*, *Phys.Rev.D* **94** (2016) 084050 [[1608.06246](#)].
- [6] A. F. Ali, S. Das and E. C. Vagenas, *The Generalized Uncertainty Principle and Quantum Gravity Phenomenology*, in *12th Marcel Grossmann Meeting on General Relativity*, pp. 2407–2409, 1, 2010, DOI [[1001.2642](#)].
- [7] K. Blanchette, S. Das and S. Rastgoo, *Effective GUP-modified Raychaudhuri equation and black hole singularity: four models*, *JHEP* **09** (2021) 062 [[2105.11511](#)].
- [8] M. A. Anacleto, J. A. V. Campos, F. A. Brito and E. Passos, *Quasinormal modes and shadow of a Schwarzschild black hole with GUP*, *Annals Phys.* **434** (2021) 168662 [[2108.04998](#)].
- [9] P. Bosso, G. G. Luciano, L. Petruzzello and F. Wagner, *30 years in: Quo vadis generalized uncertainty principle?*, *Class. Quant. Grav.* **40** (2023) 195014 [[2305.16193](#)].
- [10] P. Bosso, O. Obregón, S. Rastgoo and W. Yupanqui, *Black hole interior quantization: a minimal uncertainty approach*, [2310.04600](#).
- [11] S. Rastgoo and S. Das, *Probing the Interior of the Schwarzschild Black Hole Using Congruences: LQG vs. GUP*, *Universe* **8** (2022) 349 [[2205.03799](#)].
- [12] P. Bosso, O. Obregón, S. Rastgoo and W. Yupanqui, *Deformed algebra and the effective dynamics of the interior of black holes*, *Class. Quant. Grav.* **38** (2021) 145006 [[2012.04795](#)].
- [13] F. Fragomeno, D. M. Gingrich, S. Hergott, S. Rastgoo and E. Vienneau, *A generalized uncertainty-inspired quantum black hole*, *Phys. Rev. D* **111** (2025) 024048 [[2406.03909](#)].
- [14] D. M. Gingrich and S. Rastgoo, *Geometry of a generalized uncertainty-inspired spacetime*, *Phys. Rev. D* **111** (2025) 104017 [[2412.08004](#)].
- [15] E. T. Newman and A. I. Janis, *Note on the Kerr spinning particle metric*, *J. Math. Phys.* **6** (1965) 915.
- [16] M. Azreg-Ainou, *Regular and conformal regular cores for static and rotating solutions*, *Phys. Lett. B* **730** (2014) 95 [[1401.0787](#)].
- [17] M. Azreg-Ainou, *From static to rotating to conformal static solutions: Rotating imperfect fluid wormholes with(out) electric or magnetic field*, *Eur. Phys. J. C* **74** (2014) 2865 [[1401.4292](#)].

- [18] M. Azreg-Aïnou, *Generating rotating regular black hole solutions without complexification*, *Phys. Rev. D* **90** (2014) 064041 [[1405.2569](#)].
- [19] D. Hansen and N. Yunes, *Applicability of the Newman-Janis algorithm to black hole solutions of modified gravity theories*, *Phys. Rev. D* **88** (2013) 104020 [[1308.6631](#)].
- [20] A. Kamenshchik and P. Petriakova, *Regular rotating black hole: To Kerr or not to Kerr?*, *Phys. Rev. D* **107** (2023) 124020 [[2211.04542](#)].
- [21] W.-H. Shao, C.-Y. Chen and P. Chen, *Generating rotating spacetime in Ricci-based gravity: naked singularity as a black hole mimicker*, *JCAP* **03** (2021) 041 [[2011.07763](#)].
- [22] J. C. S. Neves and A. Saa, *Regular rotating black holes and the weak energy condition*, *Phys. Lett. B* **734** (2014) 44 [[1404.6310](#)].
- [23] EVENT HORIZON TELESCOPE collaboration, *First M87 Event Horizon Telescope Results. I. The Shadow of the Supermassive Black Hole*, *Astrophys. J. Lett.* **875** (2019) L1 [[1906.11238](#)].
- [24] EVENT HORIZON TELESCOPE collaboration, *First M87 Event Horizon Telescope Results. V. Physical Origin of the Asymmetric Ring*, *Astrophys. J. Lett.* **875** (2019) L5 [[1906.11242](#)].
- [25] EVENT HORIZON TELESCOPE collaboration, *First Sagittarius A* Event Horizon Telescope Results. I. The Shadow of the Supermassive Black Hole in the Center of the Milky Way*, *Astrophys. J. Lett.* **930** (2022) L12 [[2311.08680](#)].
- [26] E. Newman and R. Penrose, *An Approach to gravitational radiation by a method of spin coefficients*, *J. Math. Phys.* **3** (1962) 566.
- [27] U. Kumar, S. Panda and A. Patel, *Blackhole in nonlocal gravity: comparing metric from Newmann–Janis algorithm with slowly rotating solution*, *Eur. Phys. J. C* **80** (2020) 614 [[1906.11714](#)].
- [28] A. E. Balali, M. Benali and M. Oualaid, *Deflection angle and shadow of slowly rotating black holes in galactic nuclei*, *Gen. Rel. Grav.* **56** (2024) 21 [[2401.02341](#)].
- [29] V. Perlick and O. Y. Tsupko, *Calculating black hole shadows: Review of analytical studies*, *Phys. Rept.* **947** (2022) 1 [[2105.07101](#)].
- [30] S. U. Islam, J. Kumar, R. Kumar Walia and S. G. Ghosh, *Investigating Loop Quantum Gravity with Event Horizon Telescope Observations of the Effects of Rotating Black Holes*, *Astrophys. J.* **943** (2023) 22 [[2211.06653](#)].
- [31] S. Devi, A. N. S., S. Chakrabarti and B. R. Majhi, *Shadow of quantum extended Kruskal black hole and its super-radiance property*, *Phys. Dark Univ.* **39** (2023) 101173 [[2105.11847](#)].
- [32] GRAVITY collaboration, *Mass distribution in the Galactic Center based on*

interferometric astrometry of multiple stellar orbits, [Astron. Astrophys. 657 \(2022\) L12 \[2112.07478\]](#).